VSP

Journal of Adhesion Science and Technology 25 (2011) 1435–1464

Journal of ADHESION SCIENCE and TECHNOLOGY
brill.nl/jast

Adhesion Map of Spheres: Effects of Curved Contact Interface and Surface Interaction Outside Contact Region

Yin Zhang *

State Key Laboratory of Nonlinear Mechanics (LNM), Institute of Mechanics Chinese Academy of Sciences, Beijing 100190, People's Republic of China

Received in final form 26 January 2010; revised 8 December 2010; accepted 8 December 2010

Abstract

In this work three dimensionless parameters are introduced in the debate concerning hard contact models. These parameters are related to the overall adhesive contact area, curved surface contribution and surface interaction forces outside the contact region. With the variations of these three parameters, the relations and transitions between the different hard contact models such as Hertz, Bradley, Johnson–Kendall–Roberts (JKR), Derjaguin–Muller–Toporov (DMT) and Maugis–Dugdale (MD) models are presented in a systematic way. The combination of the three parameters provides a new hybrid model. The influence of these three parameters on the contact between spheres has been studied. By analyzing the pressure profiles of contact region, two new instability jumps are proposed. The instability jumps together with the three parameters are used to explain some recent experimental and numerical observations which deviate more or less from those predicated by the classical hard contact models.

Keywords

Contact mechanics, adhesion, surface interaction, instability

1. Introduction

In 1882, Hertz [1] worked out the famous contact theory relating to the contact of two elastic spheres. In 1932, Bradley [2] found that the amount of external force required to pull off two rigid spheres is $-4\pi\gamma R$ (where γ is the work of adhesion, $R = R_1R_2/(R_1 + R_2)$, and R_1, R_2 are the radii of the two spheres). In 1934, Derjaguin [3] gave a more general form for the pull-off force of two spheres separated with varying separation distance by using the approximation known as the Derjaguin approximation [4]. In 1971, Johnson, Kendall and Roberts of Cambridge University developed their famous adhesive contact model known as the JKR model [5]. In 1975, Derjaguin, Muller and Toporov [6] of Soviet Union Acad-

* E-mail: zhangyin@lnm.imech.ac.cn

DOI:10.1163/016942411X559012

emy of Sciences developed a model known as the DMT model. Heated debates over the merits of the JKR and DMT models have been exchanged for years between the English school [7, 8] and the Soviet Union school [9, 10]. The major discrepancies in the JKR model and DMT model are: (1) in the JKR contact region, there is a tensile annulus zone around the contact edge and a compressive circular zone around the center and only a compressive Hertzian pressure exists in the DMT contact region; (2) the DMT model considers the surface interaction force outside the contact region and the JKR model does not; (3) the JKR model predicts that during separation the pull-off is accompanied by an instability jump when the external load reaches $-3\pi\gamma R$ (here the negative value stands for tensile force) and the DMT model predicts a continuous separation until the point contact with the corresponding pull-off force of $-4\pi\gamma R$. In 1977, Tabor [11] noticed the neck formation during contact and the neck height, held the keys to differentiating the applicability ranges of the JKR and DMT models. Tabor defined a dimensionless number $\mu = [R\gamma^2/(E^2 z_0^3)]^{1/3}$ (where z_0 is the equilibrium separation of two half-spaces; $1/E = (1-\nu_1^2)/E_1 + (1-\nu_2^2)/E_2$, where E_1 and E_2 are the Young's moduli of the two contacting bodies; and ν_1, ν_2 are their Poisson's ratios). Physically, the Tabor number μ indicates the ratio of (the order of) neck height to z_0 [11]. In 1979 and 1980, two similar methods: the 'soft' contact method by Hughes and White [12] and the self-consistent method by Muller, Yushchenko and Derjaguin (MYD) [13] were independently proposed. The fundamental difference between the 'soft'/self-consistent methods and the classical 'hard' contact model is as follows: in 'soft' contact theory, the key concept of perfect flatness over a well-defined contact region in 'hard' contact theories is replaced by the physically consistent surface force [12]; the self-consistent method takes into account the dependence of molecular surface forces of attraction and repulsion on the distance between bodies [14]. In 1983, Muller, Yushchenko and Derjaguin conducted a computation using the Lennard–Jones (LJ) force law to describe the molecular surface interaction and the smooth transition of the pull-off force from the DMT value to the JKR value, as shown in reference [14]. In 1992, Maugis [15] used the Dugdale approximation for the force induced by the LJ potential [16] and linear elastic fracture mechanics (LEFM) approach to develop a model now known as Maugis–Dugdale (MD) model. Unlike the JKR contact pressure approaching infinity at the contact edge, the pressure inside the cohesive zone (an annulus around the contact edge) of the MD model is the theoretical stress of the material (σ_0), i.e., the maximum attractive stress due to the LJ potential. A dimensionless number called elastic number, λ ($\lambda = 1.6\mu$), was used in the MD model to show the transition between the DMT and JKR models. In 1997, Johnson and Greenwood [17] used two dimensionless parameters: $\bar{P} = P/(\pi\gamma R)$ (P: external load) and λ to construct an adhesion map, which demarcates the applicability ranges for the Hertz, Bradley, DMT, MD and JKR models. Johnson and Greenwood's adhesion map contains only the portion of $\bar{P} > 0$ and the $\bar{P} < 0$ part of adhesion map as given by Yao *et al.* [18]. Zhang's analysis on the contact pressure profile inside the contact region and the surface

interaction forces outside the contact region [19] shows the transition between the different hard contact models. However, the curved interface effect is not included in either of the references [18, 19].

Except for the Bradley model, the above classical 'hard' contact models all have a flat contact areas [19]. Flattening is not permitted in the Bradley model of rigid spheres which allows no elastic deformation [20]. A direct impact of the contact area flatness is on the calculation of the adhesion energy, which together with the elastic energy of deformation determines the final contact state [19, 21]. The experiments by Rimai *et al*. [22, 23] show that for some small particles, the 2/3 JKR power-law dependence of contact radius on particle radius is violated and an anomalous 3/4 power-law is found. Rimai *et al*. ruled out the plastic deformation causing the anomalous power-law [22, 23]. Rimai *et al*. ascribed this anomalous power-law to the curved contact interface effect [23]. From the viewpoint of the LJ force law, the contact region cannot be exactly flat because it is incommensurate with the variation of contact pressure across the area [12]. The numerical computations using the LJ potential also show the nonflatness of surface profiles in the contact region [25–27]. In 1965, Goodman and Keer [28] studied the contact of a sphere with a spherical cavity. Their computational and experimental results deviate significantly from Hertzian one due to the curved contact interface effect. However, the contact of a sphere with a spherical cavity studied by Goodman and Keer [28] is a type of *conforming* contact in which the sphere and spherical cavity fit closely together without any deformation [21]. The classical hard contact models including the Hertz, DMT, MD and JKR study the *nonconforming* contact, in which two bodies have dissimilar surface profiles [21]. In this paper two dimensionless parameters are introduced to incorporate the curvy contact interface effects of nonconforming contact.

According to Johnson and Greenwood's adhesion map [17], the JKR model applies to cases with large Tabor numbers, i.e., $\mu > 5$ (with large compliant spheres with large adhesion energy) while the DMT/Bradley model applies to case with small Tabor numbers of $\mu < 0.1$ (i.e., small hard spheres with small adhesion energy) and the MD model applies to an intermediate range of Tabor numbers. However, the following observations are found in experiments and self-consistent computations for a system with a fixed Tabor number. (1) Israelachvili *et al*. [29] found that the JKR model provides a better description of surface deformation in contact before pull-off; however, the DMT model is more accurate in predicting the pull-off force. (2) Greenwood [30] found from his self-consistent numerical simulation using the LJ force law that the force-separation curves with the relatively large fixed Tabor numbers ($\mu \geqslant 2$) are better approximated by the JKR model when the approach distance is positive (two bodies are pressed together) or slightly negative; whereas, when the negative approach distance is relatively large (i.e., with large tensile load), the curves are better approximated by the DMT/Bradley model. During separation the surfaces of the contacting bodies are found to experience a dramatic deformation in a small range of the approach distance changing sign [25, 26]. The

surface profile change results in the variations of both the total surface energy inside the contact region and surface interaction forces outside the contact region. The introduction of the three dimensionless parameters is an effort to capture and explain the above observations.

Another issue is the instability separation process called jump-off. In the JKR model, the contact radius of $a = (9\pi\gamma R^2/4E)^{1/3}$ becomes zero all of sudden at $P = -3\pi\gamma R$. In the MD model which is based on linear elastic fracture mechanics (LEFM) [15], there is a peripheral annulus zone called cohesive zone where the interface separation/failure occurs. This failure occurs by crack propagation from the contact periphery towards the center. Barenblatt [31] argues that the cracked surfaces separate continuously (as predicted by the Hertz and DMT models). It needs to be pointed out that the JKR model which uses the approach of energy balance [5, 21], according to Hui *et al.* [32], is also LEFM-based. Physically, jump-off means that the whole contact interface fails all at once rather than in a continuous way with the crack propagation. Recent theories show that when the radius of the hemispherical tip of a cylinder is small enough, the cylinder tip/substrate interface will reach strength saturation [24], i.e., become flaw-insensitive [32, 33]. Once the interface is in the flaw-insensitive regime and the external load reaches a critical tensile value, the entire interface will fail instantly, i.e., jump-off occurs. Our analysis shows that when the contact radius reduces to a critical value, the JKR/MD contact pressure distribution pattern of the peripheral tensile annulus zone and inner compressive circular zone, can no longer exist. Instead of jumping to a total separation, we propose the following two jump scenarios: (1) the JKR curve jumps to the DMT curve and the whole contact pressure thus becomes compressive. The separation then proceeds continuously, i.e., the failure mode of crack propagation holds. (2) The jump causes the whole contact pressure to become tensile and the flaw-insensitive failure mode of jump-off [24, 32, 33] will then lead to the final total separation.

The classical hard contact models (Hertz, Bradley, DMT, MD and JKR) in essence are all approximate ones and each model only applies to a certain range. Each model has its own assumptions to simplify the contact problem. The fact that the contact solution is insensitive to the nature, or say, the functional form of surface interaction provided that σ_0 and 2γ are accurately given [15, 34] also justifies such simplification. However, some important assumptions used in the hard contact models are incommensurate with the self-consistent method [35], which yields wrong predictions in hard contact models (for example, the surface force calculated by the thermodynamic approach in hard contact [36]). The thermodynamic approach [35], or say, the energy approach, is to calculate the total energy (elastic deformation energy plus the total surface energy) and then differentiate it to obtain the total surface force/tensile pressure. In the calculation of the total surface energy, for example, in the JKR model, the flatness of contact area is explicitly assumed [19, 21]. Therefore, the JKR varying contact pressure profile (also including the DMT and Hertz ones) inside a flat contact region are incompatible with the LJ force law. On the other hand, the force approach [35, 36] directly sums the local surface forces

over a gap having a preset fixed configuration, which is also the one used in the Bradley model [2]. Because surface interaction forces induce deformation (and deformation then changes the surface interaction forces), the force approach violates the self-consistent rules by presetting a fixed configuration [35, 36]. The thermodynamic approach and force approach in hard contact can lead to two different predictions on the surface forces as demonstrated by Muller *et al*. [35] and Pashley [36]. The reason causing the surface force difference calculated by the thermodynamic approach and force approach in hard contact is that these two approaches preset the different sphere surface profiles instead of allowing the system to come to an equilibrium profile in a minimum energy configuration [35, 36]. In contrast, the self-consistent method ignores those assumptions of presetting contact body surface profile and offers a much more refined way of computing the contact problem by using the LJ potential. In a self-consistent method, the thermodynamic approach and force approach give completely equivalent results [35]. However, the mathematical handling of singular integrand, path-grabbing numerical method, the 'appalling' convergence rate and large amount of computation [30] required/encountered in a self-consistent method are, by any standard, a daunting job to a researcher. The three dimensionless parameters in this paper are introduced to: (1) capture the deviations as observed in both experiments and self-consistent methods; (2) thus offer better approximations; (3) more importantly, keep the beauty of simplicity of the classical hard contact models.

2. Surface Interaction Force and Derjaguin Approximation

The following derivation on the total surface interaction force is the force approach, which gives correct force value as compared with the thermodynamic approach [36].

If $\sigma(h)$ is the surface interaction force per unit area, the total surface force outside the contact area, P_{vdW}, can be summed up as follows [36]:

$$P_{\mathrm{vdW}} = \int \sigma(h)\,\mathrm{d}A = \int_a^\infty \sigma(h)\,\mathrm{d}(\pi r^2), \tag{1}$$

where a is the contact radius and h is the separation distance. If the parabolic approximation is used for the spheres surface profiles, i.e., $h = r^2/2R$, equation (1) becomes:

$$P_{\mathrm{vdW}} = 2\pi R \int_z^\infty \sigma(h)\,\mathrm{d}h. \tag{2}$$

For the LJ force law, $\sigma(h)$ is given as follows [4, 25, 26, 30]:

$$\sigma(h) = \frac{16\gamma}{3z_0}\left[\left(\frac{z_0}{h}\right)^3 - \left(\frac{z_0}{h}\right)^9\right]. \tag{3}$$

Again, 2γ is the work of adhesion and z_0 is the equilibrium separation of two half-spaces in the LJ surface force law [37]. Here the positive value of σ indicates attraction and the negative is repulsion. The maximum attractive $\sigma(h)$ is

$\sigma_0 \approx 1.03 \times 2\gamma/z_0$ at $h \approx 1.255 z_0$. The term σ_0 is often referred to as the theoretical stress of materials or cohesive strength. Substitute equation (3) into equation (2), we have:

$$P_{\mathrm{vdW}}(z) = 4\pi R\gamma \left[\frac{4}{3}\left(\frac{z_0}{z}\right)^2 - \frac{1}{3}\left(\frac{z_0}{z}\right)^8 \right]. \tag{4}$$

During the integration of equation (2), z is treated as a given fixed value [4]. Therefore, equation (2) physically gives the interaction forces of two flat surfaces. The Derjaguin approximation states that the interaction energy/force between small areas of (slightly) curved solids can be (accurately) approximated by the interaction energy/force of two flat surfaces [4, 30]. Physically, the 3–9 force law of $\sigma(h)$ in equation (3) is the surface force per unit area of two flat half-spaces separated by a distance h, which is derived from the 6–12 LJ potential law for two isolated molecules [37, 38]. In many self-consistent computations [26, 27, 30], equation (3) is used as the local pressure of a curved contact interface. So, in that sense, besides equation (4) which expresses the total surface force, equation (3) is also referred to as the Derjaguin approximation [38]. From the point of view of elasticity, $\sigma(h)$ is a normal surface traction [37]. Instead of using the Derjaguin approximation of equation (3), Argento *et al*. [39] derived the surface traction by directly summing up the body forces of molecules as given by the LJ 6–12 potential through a double volume integration. Argento *et al*. [39] also showed that when (at least) one contacting body is a half-space, the Derjaguin approximation which ignores the surface profile and is usually regarded as an approximation, in fact gives the exact total surface force. However, Wu [38] demonstrated by using Argento's approach [39] that when the sphere radius is very small (comparable with z_0 and the commonly accepted z_0 value is 0.4 nm [26]) or the Tabor number is large, the Derjaguin approximation of equation (3) is not accurate in the contact of a rigid sphere with an elastic half-space. While, when the sphere is very small, problems concerning the validity of the continuum theory will arise [37].

The maximum attractive surface interaction force obtained from equation (4) is $P_{\mathrm{vdW}} = 4\pi R\gamma$ at $z = z_0$. The tensile external load required to balance the attractive surface interaction force is thus $P = -P_{\mathrm{vdW}}$ and the maximum tensile external load is $-4\pi R\gamma$, which is the DMT pull-off force. Here it needs to be emphasized, that P_{vdW} is the surface force outside the contact area and the equilibrium equation of $P = -P_{\mathrm{vdW}}$ can only be valid for two cases: (1) the Bradley model (there is no contact region for two rigid spheres, i.e., $a = 0$. z is 'the nearest distance between the centers of surface molecules of the spheres' [2], and therefore P_{vdW} of equation (4) is the only force for an external load to balance); (2) for the DMT model at the point of separation (for the DMT model, the spheres separate at $a = 0$ and therefore there is no force contribution from the contact region at that critical point), the equation of $P = -P_{\mathrm{vdW}}$ does not deal with any elastic deformation, which is also often referred to as the Bradley model [30]. The JKR pull-off force of $-3\pi R\gamma$ can be obtained by setting $z \approx 1.3 z_0$ in equation (4). Although the JKR pull-force of

$-3\pi R\gamma$ and the DMT pull-force of $-4\pi R\gamma$ differ by 33%, both imply that the pull-off force scales linearly with γ and is independent on the Young's moduli of contacting spheres. The linearity dependence of pull-off force on γ is demonstrated, to good approximation, by a self-consistent model [25]. However, because there is elastic deformation in both the JKR and DMT models, the sphere pull-off forces independence on Young's moduli is puzzling [15]. For conical and flat-ended cylinder indenters, the pull-off force is dependent on the Young's modulus [40]. Muller, Yushchenko and Derjaguin [13, 14] and Maugis [15] showed the smooth transition of the sphere pull-off force from $-4\pi R\gamma$ at $\mu = 0$ to $-3\pi R\gamma$ at $\mu = \infty$ (the different dimensionless parameters used by Muller, Yushchenko and Derjaguin [13, 14] and Maugis [15] are the Tabor number μ with different numerical factors [30]).

To derive equation (4), the parabolic approximation of surface profile and the Derjaguin approximation are used. These two approximations in essence violate the self-consistent rule by presetting the surface profiles. Therefore, it is not surprising that the larger tensile pull-off force ($P < -4\pi R\gamma$) can be derived by other methods. For example, Attard and Parker [25] show in their Fig. 7 that the pull-off force obtained by a self-consistent method reaches the minimum of about $0.8 \times (-4\pi R\gamma)$ (their γ and our γ differed by a factor of 2); and their pull-off seems to increase indefinitely with the increase of the dimensionless parameter σ. The dimensionless parameter σ defined by Attard and Parker is shown to be related to the Tabor number (μ) as $\sigma = 0.5\mu^{3/2}$ [30]. However, Greenwood's self-consistent method together with others (in his Fig. 7) [30] shows that this $-4\pi R\gamma$ is the upper limit of the pull-off force.

3. Contact Pressure, Adhesion Energy and Equilibrium

The contact pressure profile in the JKR model is assumed to have the following form [21]:

$$p(r) = p_0(1 - r^2/a^2)^{1/2} + p_0'(1 - r^2/a^2)^{-1/2}. \tag{5}$$

The first term of $p_0(1 - r^2/a^2)^{1/2}$ is the compressive Hertz pressure; the second term of $p_0'(1 - r^2/a^2)^{-1/2}$ is a tensile one, which is often referred to as the Boussinesq pressure. The negative p_0' value is, so far, unknown. The positive p_0 is found by an elasticity approach of solving a Boussinesq problem, which has the following expression [21]:

$$p_0 = \frac{2Ea}{\pi R}. \tag{6}$$

The pressure inverse square root singularity at the contact edge ($r = a$) is given by equation (5). This singularity is the Mode I characteristic of an interface crack between an incompressible elastic solid and a rigid solid [32]. Therefore, the contact problem is often treated as contacting bodies with circumferential cracks [15, 24]. Here Griffith's concept of energy release rate for brittle materials [41] is applied to find the negative tensile pressure p_0'.

Let γ_1 and γ_2 be the surface tensions of two surfaces before contact, and γ_{12} be the interface tension after contact. Usually, $\gamma_1 + \gamma_2 > \gamma_{12}$, which is to say that when two surfaces unite to form an interface, the net free energy is reduced. This energy reduction, often known as the Dupré work of adhesion [42], is:

$$2\gamma = \gamma_1 + \gamma_2 - \gamma_{12}. \tag{7}$$

In an adhesive contact, the total free energy consists of two parts: the elastic energy and the adhesion energy inside the contact area, i.e., $U_T = U_E + U_S$. The elastic energy due to deformation is calculated as follows [21]:

$$U_E = \frac{\pi^2 a^3}{E}\left(\frac{2}{15}p_0^2 + \frac{2}{3}p_0 p_0' + p_0'^2\right), \tag{8}$$

where p_0 and p_0' also have the following relation [21]:

$$\delta = \frac{\pi a}{2E}(p_0 + p_0'). \tag{9}$$

Herer δ is the approach of the center of sphere with respect to the zero force position of $h = z_0$ [30]. In conjunction with equations (6) and (9), p_0' is found to be:

$$p_0' = \frac{E}{\pi}\left(\frac{\delta}{a} - \frac{a}{R}\right). \tag{10}$$

Substituting equations (6) and (10) into equation (8), the elastic energy U_E now becomes:

$$U_E = E\left(\frac{a^5}{5R^2} - \frac{2}{3}\frac{\delta a^3}{R} + a\delta^2\right). \tag{11}$$

For a fixed δ, $\partial U_E/\partial a$ is:

$$\frac{\partial U_E}{\partial a} = Ea^2\left(\frac{a}{R} - \frac{\delta}{a}\right)^2 = \frac{\pi^2 a^2}{E}p_0'^2. \tag{12}$$

Before we start the calculation of the total surface energy inside contact region (adhesion energy), it is necessary to have a discussion on the flatness of the contact region. The contact region with the pressure profile given in equation (5) is flat from an elastic point of view [19]. Here we just give a brief description. The compressive Hertz pressure of $p_0(1 - r^2/a^2)^{1/2}$ generates a parabolic displacement and the tensile Boussinesq pressure of $p_0'(1 - r^2/a^2)^{-1/2}$ generates a constant/translational displacement. If the surface profile of an un-deformed sphere is approximated to a parabola as given above, the parabolic displacement due to the Hertz contact pressure will cancel exactly the curviness of the un-deformed bodies and make the contact region flat. Because the Boussinesq pressure only generates a constant displacement, the contact surface shapes of nonadhesive (Hertz) contact and adhesive (JKR) contact should be the same. However, the fringes of equal chromatic order (FECO) images by Israelachvili *et al.* [29] show differently: the surface configuration of Hertz contact bifurcates more smoothly; the JKR bifurcates very sharply

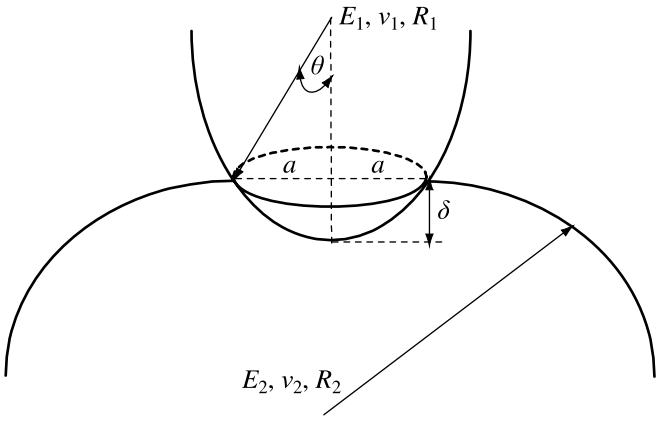

Figure 1. Schematic diagram of the contact of two elastic spheres and related parameters.

and the contact region looks flat. Muller *et al*. expressed their puzzlement on this experimental observation [35]. The term $p(r)$ of equation (5) varies monotonously inside the contact region and physically, the pressure is induced by the LJ force law of equation (3). The contact region thus cannot be (exactly) flat according to the self-consistent rule because, otherwise, the contact pressure would be constant inside a flat contact region according to equation (3).

In general, as shown in Fig. 1, the contact interface is assumed to be a curved one rather than a flat one. Therefore, A_{cs}, the area of the curved surface in contact, is approximated to a part of a spheroid surface rather than a flat one of πa^2 as follows:

$$A_{cs} = \pi(a^2 + \Delta^2) = \pi a^2\left(1 + \frac{a^2}{4R^2}\right), \tag{13}$$

where Δ is defined as $\Delta = R - \sqrt{R^2 - a^2} \approx a^2/2R$. The total surface energy of the curved contact area can now be written as:

$$U_S = -2\gamma J A_{cs} = -2\gamma J \pi a^2\left(1 + \frac{a^2}{4R^2}\right). \tag{14}$$

Here J is a dimensionless number. Physically, J is the ratio of effective adhesive contact area to A_{cs}. There are two major reasons for adding this J parameter. Firstly, A_{cs} is just a nominal geometric area. To have the adhesive contact area equal to the geometric area, the surfaces of two contact bodies must be 'molecularly smooth' [11]. In reality, the adhesive contact area is not equal to the geometric area because of the roughness. Secondly, A_{cs} is the area of a spheroid surface part, which in essence is used as an approximation for the real contact area. There is no mechanism to guarantee that the curved contact surface under different P and γ will keep the surface shape of a spheroid. As shown in Attard and Parker's Fig. 6(a) presented by a self-consistent method [25], the contact surface profile is almost flat when the approach h_0 is negative (h_0 is the separation distance between two centers of contacting bodies; negative h_0 corresponds to positive δ, which physically

means that two bodies are pressed together [25]) though a closer view reveals that it is not exactly flat. The flat contact area is indeed a good approximation for this scenario. However, when h_0 is positive, the contacting surface profile becomes very curved and thus the flat contact area approximation is not appropriate any more. From Attard and Parker's Fig. 6(a) [25], the contact surface profile experiences only one dramatic shape change in a narrow range of h_0 changing from negative values to positive values: a flat one of negative h_0 and a curved one of positive h_0. There are no obvious contact surface shape changes in both the $h_0 > 0$ range and the $h_0 < 0$ range. The terms h_0 and δ are dependent on the external load, for example, a large positive δ value or a large negative h_0 value corresponds to large compressive external load. The sign changes of h_0 and δ are closely related with the compressive/tensile change of the external load. It suggests that the external load is a dominant factor in determining J. At the same time, Young's moduli of the spheres may also have an influence on J. When two spheres have similar Young's moduli, two J values in general should be used: one for the compressive external load case to ensure a flat contact area, i.e., $JA_{\mathrm{cs}} = A_{\mathrm{flat}} = \pi a^2$; the other for the tensile external load case to describe the curved contact surface. However, for a rigid glass particle in contact with the highly compliant polyurethane substrate [22, 23], only one J value should be taken into account for the curved contact interface effect.

The equation (12) by Rimai *et al*. [23] is:

$$\mathrm{d}A_{\mathrm{cs}} = \frac{\mathrm{d}A_{\mathrm{flat}}}{\cos\theta} = 2\pi\sqrt{\frac{R^2}{R^2 - a^2}}a\,\mathrm{d}a. \tag{15}$$

Here $\cos\theta = \sqrt{R^2 - a^2}/R$ and θ is the angle shown in Fig. 1. This equation (15) in essence is to account for the curved contact interface effect by transforming a (differential) flat contact area into a (differential) spheroid area, which in our case is defined by $J = 1$. Once again, the parabolic approximation of un-deformed spheres is the reason for predicting the flatness of contact area. When a/R is small, the parabolic approximation works fine [21]. When $a/R > 0.4$, the parabolic approximation for the sphere surface profile and linear elasticity, no longer holds [37]. The exact expression for the spherical surface profile is required for the adhesion strength computation [24] and the large contact radius case [43]. The parabolic approximation assumed in the JKR, DMT and MD models also results in the incorrect prediction that the adhesive strength can surpass the largest possible theoretical strength as the size of sphere radii reduces [24]. Clearly in equation (13) $\frac{a^2}{4R^2}$ is a second order term when a/R is small, which should be ignored at first. However, keep in mind that the curved contact interface also changes J and as shown later this curved contact interface can have a significant influence on the contact state. For equilibrium, the Griffith criterion requires $\partial(U_{\mathrm{E}} + U_{\mathrm{S}})/\partial a$ to vanish, giving:

$$\frac{\pi^2 a^2}{E}p_0'^2 = -\frac{\partial U_{\mathrm{S}}}{\partial a} = 4\pi J\gamma a\left(1 + \frac{a^2}{2R^2}\right). \tag{16}$$

Therefore:

$$p_0' = -\sqrt{\frac{4JE\gamma}{\pi a}\left(1 + \frac{a^2}{2R^2}\right)}. \tag{17}$$

The minus sign is chosen to let p_0' be tensile.

The following amount of external load P is required to balance the force due to elastic deformation:

$$P = \int_0^a 2\pi r p(r)\,\mathrm{d}r = \left(\frac{2}{3}p_0 + 2p_0'\right)\pi a^2. \tag{18}$$

The above equation only sums the forces inside the contact region, which is the JKR case. For the DMT case which corresponds to the small Tabor number case and thus has small 'neck' height, the surface interaction force outside the contact area cannot be ignored. The surface interaction force acts like an additional external load [44] and equilibrium is reached when the elastic restoring force balances the combined effect of surface force and external load [36]. Equation (18) is thus written as follows to include the surface interaction force outside the contact region:

$$P + P_{\mathrm{vdW}} = \left(\frac{2}{3}p_0 + 2p_0'\right)\pi a^2. \tag{19}$$

Here P_{vdW} is given by equation (1). Equation (19) also offers us a framework to show how different classical hard contact models are related:

Bradley model: Because there is no elastic deformation for rigid spheres, $p_0 = p_0' = 0$, the equation (19) recovers the Bradley model.

Hertz model: Because it involves a nonadhesive contact, P_{vdW} of the surface interaction force outside the contact region and p_0' induced by the adhesion, are both zero. When $P_{\mathrm{vdW}} = p_0' = 0$, equation (19) recovers the Hertz model (in conjunction with equation (6)).

DMT model: $p_0' = 0$ because in the DMT model there is no tensile pressure inside the contact region. Because of its short 'neck', the surface interaction forces outside the contact region is accounted for. So when $p_0' = 0$ and P_{vdW} is taken with the maximum value of $P_{\mathrm{vdW}} = 4\pi R\gamma$, equation (19) recovers the DMT model (in conjunction with equation (6)).

JKR model: Because a flat contact area is formed, equation (17) is thus modified as $p_0' = -\sqrt{\frac{4E\gamma}{\pi a}}$. Also because of its large 'neck' height, the surface interaction force outside contact region can be ignored. So when $p_0' = -\sqrt{\frac{4E\gamma}{\pi a}}$ and $P_{\mathrm{vdW}} = 0$, equation (19) recovers the JKR model (in conjunction with equation (6)).

The MD model is expressed by two coupled equations [15], which cannot be recovered by equation (19). The MD pull-off force is between the JKR one and DMT one [15, 19, 44].

In conjunction with equations (6) and (17), equation (19) now gives the force-contact radius curve, after some simple manipulations as:

$$\left(P-\frac{4Ea^3}{3R}\right)^2 = 16\pi J E\gamma a^3\left(1+\frac{a^2}{2R^2}\right) + 4\pi a^2 P_{\mathrm{vdW}}\sqrt{\frac{4JE\gamma}{\pi a}\left(1+\frac{a^2}{2R^2}\right)} + P_{\mathrm{vdW}}^2. \tag{20}$$

The equation (20) presents the P–a curve. From the viewpoint of self-consistent method, the contact radius is an ill-defined concept [25–27]. The physical meanings of contact radius for different contact models are also different, for example, at the contact edge, the pressure of the Hertz model drops to zero and the pressure of the JKR model goes to infinity at the contact edge [19]. In the self-consistent method, it is the force-approach (P–δ) curve that is used and that is presented in references [25–27, 30]. Experimentally, measuring the normal displacement δ is also much easier than measuring the contact radius a [45]. However, many theoretical analysis [1, 5, 6, 15, 28] and experiments [5, 22, 28, 29, 46] are done using the P–a curves. This paper adopts the P–a curve approach for comparison purposes. The conversion of P–a curves to P–δ curves can be done through the δ–a relationship given by Maugis [15].

The following two dimensionless quantities are introduced to nondimensionalize equation (20):

$$F=\frac{P}{P_{\mathrm{c}}}, \qquad A=\frac{a}{a_{\mathrm{c}}}, \tag{21}$$

where $P_{\mathrm{c}}=3\pi R\gamma$ and $a_{\mathrm{c}}=(9\pi R^2\gamma/4E)^{1/3}$ and $(-P_{\mathrm{c}})$ and a_{c} are the pull-off force and radius, respectively of the JKR model when P is the control parameter [21]. The dimensionless form of equation (20) is as follows:

$$(F-A^3)^2 = 4JA^3(1+\beta A^2)+\frac{16}{3}\kappa\sqrt{J(1+\beta A^2)}+\frac{16}{3}\kappa^2. \tag{22}$$

The dimensionless numbers β and κ are defined, respectively, as follows:

$$\beta=\frac{3}{4}\left(\frac{3\pi}{2}\right)^{1/3}\left(\frac{1}{R^2}\frac{\gamma^2}{E^2}\right)^{1/3}=\frac{3}{4}\left(\frac{3\pi}{2}\right)^{1/3}\mu\frac{z_0}{R}, \qquad \kappa=\frac{P_{\mathrm{vdW}}}{4\pi R\gamma}. \tag{23}$$

Again, $\mu=[R\gamma^2/(E^2z_0^3)]^{1/3}$ in the above equation is the Tabor number. The equation (22) offers a hybrid model of accounting for the effects of both the curved contact interface and the surface interaction forces outside the contact region. The terms J, β and κ are dependent on external load, adhesion energy, Young's modulus, surface asperity, contact body geometry, etc. Or in other words, they are dependent on the elastic deformation of the contacting bodies: J and β are used to capture the curviness of the contact region, which has a direct impact on the total surface energy; κ indicates the surface interaction forces outside the contact region and is directly related to the neck formation. Note, a large Tabor number means a

large neck height and thus a small κ. In the small h_0 (or δ) sign-changing range accompanied by the dramatic surface profile change as observed in [25, 26], it is possible for J, β and κ to vary dramatically and at the same time, continuously. How to capture these three parameters variations in that small h_0 (δ or external load) sign-changing range is beyond the scope of this paper. The terms J, β and κ here are treated as constants to show how they influence the contact.

Once again, here we show how the different contact models are obtained with the variations of J, β and κ in equation (22). When $J = \kappa = 0$, the Hertz model of $F = A^3$ is obtained. When $J = 1$ and $\beta = \kappa = 0$, the JKR model of $(F - A^3)^2 = 4A^3$ is obtained. The JKR model can also be obtained by setting $J = 1/(1 + \beta A^2)$ ($\beta \neq 0$) and $\kappa = 0$. The physical meaning of setting $J = 1$ and $\beta = \kappa = 0$ is clear: a flat contact area and zero surface interaction force outside contact region. The physical meaning of $J = 1/(1 + \beta A^2)$ is so far not clear to us. In equation (22), the term $4JA^3(1 + \beta A^2) + \frac{16}{3}\kappa\sqrt{J(1 + \beta A^2)}$ is due to the tensile pressure of p_0', and it vanishes with the assumption of Hertzian contact pressure. The equation (22) thus becomes:

$$F = A^3 - \frac{4}{3}\kappa. \tag{24}$$

When $\kappa = 0$ we have the Hertz model and when $\kappa = 1$ we have the DMT model. So physically, it is clear that the DMT model simply superimposes the surface interaction forces as an additional external load to the Hertz model. For rigid spheres there is no elastic deformation and thus zero contact radius ($A = 0$), and equation (24) becomes the Bradley model of $F = -\frac{4}{3}\kappa$.

The above statement is summarized in Fig. 2. Unlike the adhesion map presented by Johnson and Greenwood [17], which indicates the applicability ranges of the different contact models, the main idea of Fig. 2 is to show how different contact models relate and transit to one another in a clear mathematical way by varying these three parameters.

Now let us examine how J and β influence the contact (κ is thus set as zero for the time being). Figure 3 shows the F–A curves with different J and β values. Clearly, for fixed F and β, the larger is J the larger is A. Also for fixed F and J, the larger is βth larger is A. Physically, with the value of 2γ fixed, larger values of J and β gives greater (negative) total surface energy and larger tensile pressure inside contact area as indicated in equations (14) and (17), which as a consequence pulls more body parts into contact. As noticed in Fig. 3, $J = 0$ is the Hertz model; $J = 1$ and $\beta = 0$ is the JKR model. In Fig. 4, J is fixed as 1 and β varies from 0 to 0.3. Again, for a given load F, the larger is β the larger is the contact radius A. The pull-off force is, by definition, the tensile force required to separate two contacting bodies, which is also the maximum tensile force [14, 36]. The pull-off points are marked with a circle in Fig. 4. At $\beta = 0$, the pull-off force is $F_{\text{pull-off}} = -1$ of the JKR model and the pull-off force increases with β. At $\beta = 0.3$, $F_{\text{pull-off}} = -1.44$, which exceeds the DMT pull-off force of $-4/3$. Here we must emphasize that J and β are two phenomenological parameters used to capture the curved contact

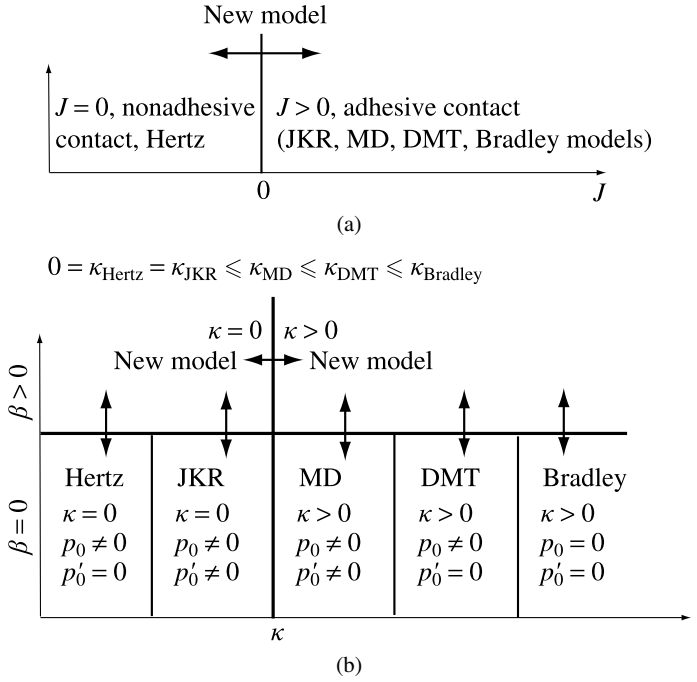

Figure 2. Adhesion maps on the transition of the different contact models.

interface effect. So far, we do not know in details how they vary with the external load, adhesion energy, contact body geometries, etc. The variations of β in Fig. 4 demonstrate that the curved contact interface effect can be a mechanism with the capability to cover the pull-off force transition from the JKR value to the DMT value. This is a different transition mechanism from the previous ones [13–15], in which the pull-off force transition is shown with the variation of the Tabor number (with different numerical factors). The dimensionless Tabor number, μ, indicates the ratio of (the order of) neck height to z_0 [11]. The Tabor number thus determines whether or how much surface interaction force should be taken into account, for example, $P_{\mathrm{vdW}} = 0$ for the JKR model and $P_{\mathrm{vdW}} = 4\pi R\gamma$ for the DMT model. In both the JKR and DMT contacts, the contact area is flat. Now let us have a dimensional analysis on β defined in equation (23). Clearly β is due to the $a^2/2R^2$ term in equation (20). Ignoring the numerical factor, we have $\beta = \mu\frac{z_0}{R}$. μ is the Tabor number and z_0/R is the size ratio, which are two independent basic variables used in the nanoscale contact mechanics study [37, 38]. Therefore, either large μ or large z_0/R gives a nontrivial β value.

It is also interesting to notice that in the experiments done by Horn *et al.* [46], all their measured contact radii are larger than that predicted by the JKR model, which resemble the dashed and dotted curves of $\beta \neq 0$ in our Fig. 4. Israelachvili *et al.* [29] also observed that though the JKR model better describes the surface deformation in contact before pull-off, the pull-off force is found to be more consistent with the

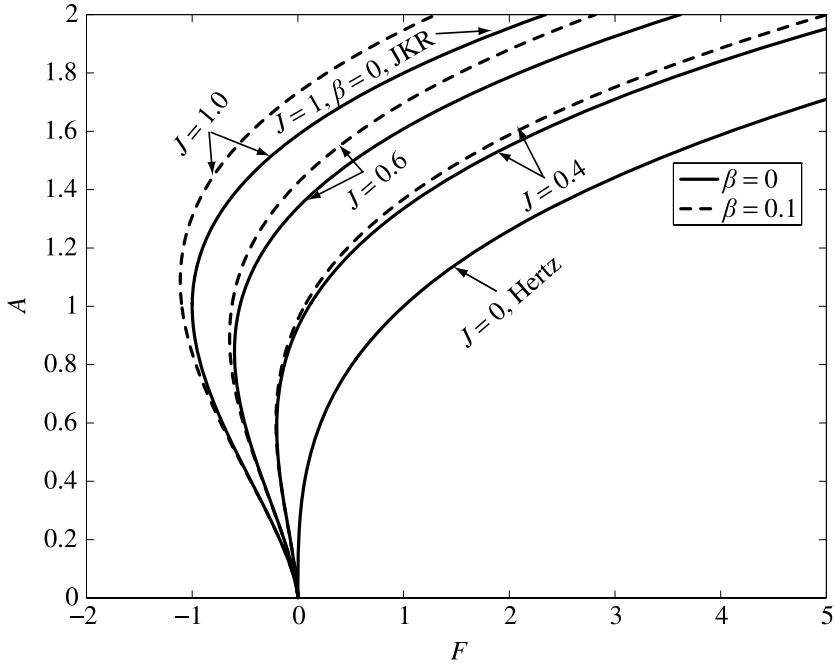

Figure 3. The evolution of the F–A curves as J changes. Here two groups of $\beta = 0$ (solid lines) and $\beta = 0.1$ (dashed lines) are studied. $J = 1$ and $\beta = 0$ is the JKR contact model and $J = 0$ is the Hertz contact model.

DMT value. The curved contact interface effect can offer an explanation for that. As shown in their Fig. 6(a) by Attard and Parker [25], when two bodies are pressed tightly (negative h_0), their contact interface profile is almost flat (our $J = 1$ and $\beta = 0$ case and the JKR model); when two bodies are pulled away from each other (positive h_0), the contact interface profile (suddenly) becomes very curved, which results in the (sudden) increase of β and thus a larger pull-off force closer to the DMT value. The plots of the pull-off force and radius as the functions of J and β are shown in Figs 5 and 6, respectively. Because the pull-off force is always tensile (negative value), in Fig. 5, the pull-off force monotonously decreases with J and β. In other words, the curved contact interface effect results in a larger tensile pull-off force. On the other hand, the pull-off radius in Fig. 6 monotonously increases with J and β.

Another possible issue caused by the curved contact interface is the anomalous power-law dependence of the contact radius on the particle radius under zero external load observed by Rimai *et al.* [22, 23]. In their experiments of soda-lime glass particle contact with a highly compliant polyurethane substrate, Rimai *et al.* [22, 23] showed that the power-law exponents of some particles is 3/4 rather than 2/3 predicted by the JKR model. Because of the rigid-soft contact, the contact interface is supposed to be a curved one as indicated by equation (15) [23]. Rimai *et al.* humbly call their analysis 'superficial': the introduction of equation (15) does

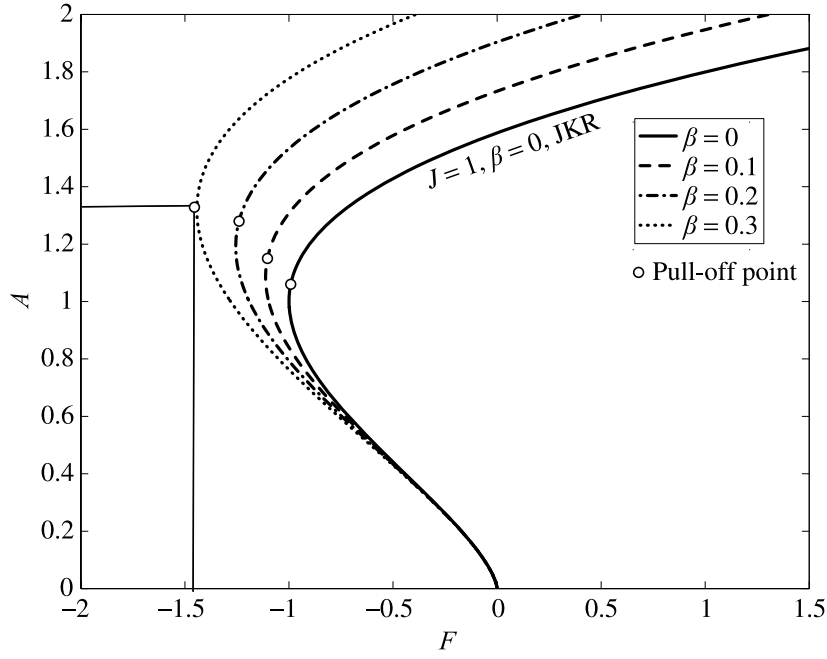

Figure 4. The evolution of the $F-A$ curves as β changes from 0 to 0.3 and J is fixed as 1. The solid line is the JKR contact model.

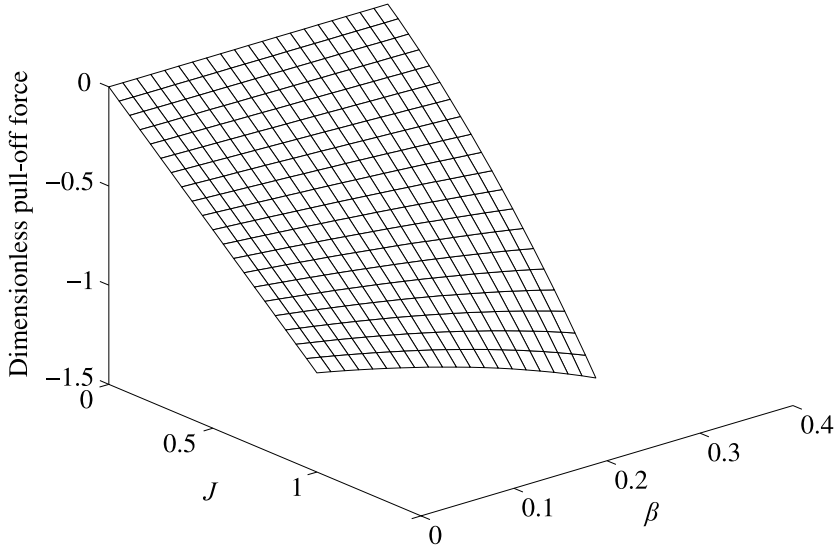

Figure 5. Plot of the dimensionless pull-off force as the function of J and β.

explain the anomalous 3/4 power-law exponent phenomenon, however, the major drawback in their model as pointed out by themselves is that the tensile contact pressure is not accounted for [23].

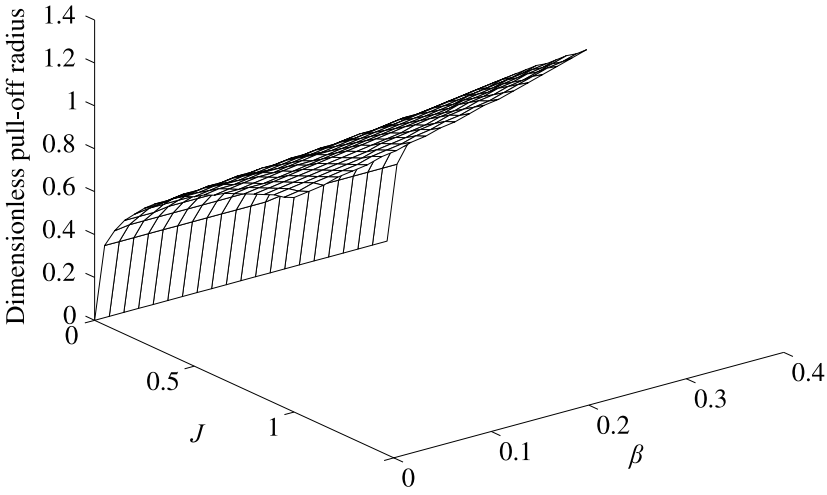

Figure 6. Plot of the dimensionless pull-off radius as the function of J and β.

Now, we introduce both the tensile pressure and curved contact interface effects to see how the power-law exponent can be influenced. For the convenience of comparison, the dimensional governing equation of equation (20) is used and by setting $P_{\mathrm{vdW}} = 0$, it becomes:

$$\left(P - \frac{4Ea^3}{3R}\right)^2 = 16\pi J E\gamma a^3\left(1 + \frac{a^2}{2R^2}\right). \tag{25}$$

The derivation of the above equation uses equation (5) and the tensile pressure is thus incorporated. If the curved contact effect is eliminated, equation (25) becomes the JKR model as:

$$\left(P - \frac{4Ea^3}{3R}\right)^2 = 16\pi E\gamma a^3. \tag{26}$$

When $P = 0$, equation (26) leads to the following relation of the contact radius under zero external load: $a_0 = (\frac{9\pi\gamma}{E})^{1/3}R^{2/3}$, which is the JKR 2/3 power-law.

Equation (25) becomes as follows when $P = 0$:

$$a_0^3 = \frac{9\pi J\gamma}{E}R^2\left(1 + \frac{a_0^2}{2R^2}\right). \tag{27}$$

In the experiment, $\gamma \approx 0.04$ J/m^2 and E is in the range between 3×10^6 Pa and 5×10^6 Pa [22]. Therefore, $9\pi\gamma/E$ is about 0.32–0.5 μm. In Fig. 7, we set $M = 9\pi\gamma/E$ as 0.3 μm, 0.5 μm and 2.66 μm, respectively. The reason for setting $M = 2.66$ μm is that $a_0 \approx R$ when $M = 2.66$ μm and a larger M will lead to the unrealistic result of $a_0 > R$. Here R is taken as 3.8 μm, 10.1 μm, 21.1 μm, 43.9 μm, 60.6 μm and 101.7 μm [22], respectively. The least-square method was applied to curve-fit the $\ln(R)$–$\ln(a_0)$ data points derived from equation (27) as a straight line of $k_1x + k_2$. Clearly, the slope k_1 in Fig. 7 has no significant change and the JKR

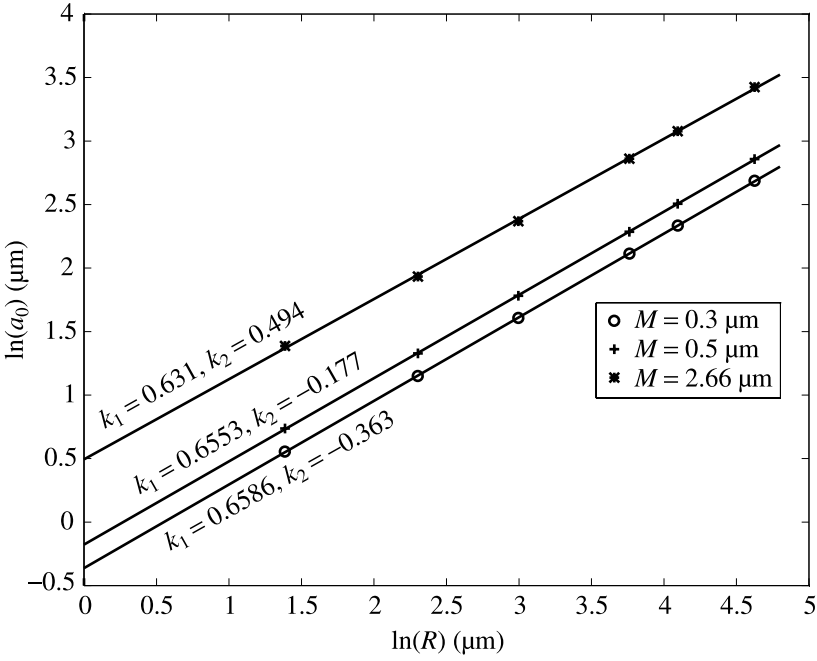

Figure 7. $\ln(R)$–$\ln(a_0)$ plot of a rigid particle contact with a compliant substrate. M is defined as $M = 9\pi\gamma/E$ and a straight line of $k_1 x + k_2$ is used for curve-fitting.

2/3 power-law works fine in this relatively large range of M. In contrast to the conclusion by Rimai *et al*. [23], the curved contact interface effect in our study does not have any significant impact on the JKR 2/3 power-law. It is also worth mentioning that some particles still obey the JKR 2/3 power-law in Rimai's experiments [23]. The JKR model is derived from the linear elasticity of the half-space model and it thus only applicable to the scenario that the contact radius is small compared to the contacting body dimensions [21]. Johnson also explicitly states that the JKR model is established for two similar homogeneous solids [47], not for the soft-hard contact scenario. In the Rimai's experiments [22, 23], the compliant substrate almost engulfs half of the hard glass particle and a large elastic or even plastic deformation may occur in the substrate. The plastic deformation which leads to an 1/2 power-law relation [48] is excluded as a reason causing the anomalous 3/4 power-law [22, 23]. The large meniscus height in Rimai's experiments [22, 23] is noticed, which causes sharp surface shape changes at the edge of contact region. This, according to Tabor [11], involves a large elastic strain and the classical linear elasticity cannot be strictly applied, which could be the reason causing the anomalous power-law.

We now examine how the surface interaction force P_{vdW} influences the contact. Therefore, we set $J = 1$ and $\beta = 0$ in equation (22) and the following equation is obtained after some simple manipulations:

$$F = A^3 - \sqrt{4A^3 + \frac{16}{3}\kappa + \frac{16}{9}\kappa^2}. \tag{28}$$

Physically, equation (28) retains the JKR pressure of equation (5) and recovers the JKR model when $\kappa = 0$.

The JKR model assumes that the attractive forces are confined in the contact region and zero outside.

The attractive forces results in the tensile contact pressure of $p_0'(1 - r^2/a^2)^{-1/2}$ of equation (5) and this tensile contact pressure produces a constant displacement, which is to form a neck. If the neck height is large (compared with z_0), the surface interaction force outside the contact region can be ignored. In comparison, the DMT model assumes that all the attractive forces act outside the contact region and there is only a compressive contact pressure inside the contact region. Tabor argues [11] that when considering the surface interaction outside the contact region, the attractive surface force around the contact edge is so large that some extra surfaces must be pulled in the contact. A tensile contact pressure must exist inside the contact region to form a neck to reduce/insulate the attractive surface interaction force. Otherwise, the attractive surface interaction force around the contact edge will continue to pull more surface into contact forever. Also, in the viewpoint of fracture mechanics [15, 24, 32, 33], an annulus of tensile cohesive zone around the contact edge is needed to start the crack propagation. On the other side, the JKR model ignores the surface interaction force outside contact region, and therefore, may not be applicable when the contact area is small [33]. Horn *et al.* [46] experimentally observed that their measured data with small contact radii around the pull-off point do not fit the JKR curve in an adhesive contact though their data does fit the Hertz curve fairly well in a nonadhesive contact experiment. We call equation (28) the hybrid equation which includes the attractive forces both inside and outside the contact region.

Figure 8 presents the hybrid equation with $\kappa = 0.1$, $\kappa = 0.3$, the JKR and DMT models respectively. The curves of the hybrid equation are both above the JKR curve, which, again, is consistent with the experimental observation in reference [46]. The surface interaction forces outside the contact region and the curved contact interface both result in a larger contact radius. It is also noticed in Fig. 8 that the hybrid equation closely matches the JKR model when the compressive external load is relatively large; the difference only becomes larger in the tensile range of the external load. Therefore, the hybrid equation is a modification and answer to Tang's concern that the JKR model may not be applicable in the small contact radius case around the pull-off point [33]. The pull-off points are marked with a square, a triangle and a circle, respectively. The pull-off force at $\kappa = 0.3$ is the same as the DMT one ($F = -4/3$) and further increasing κ will lead to larger pull-off force than the DMT one. The term $\kappa = \frac{P_{\mathrm{vdW}}}{4\pi R\gamma}$ is defined in equation (23). R and γ are fixed for a given system. The reason for the κ variation is due to P_{vdW}. The term P_{vdW} of equation (4) is a function of z and physically, z is the separation distance at the contact edge and z varies for different contact models because of the neck formation at the contact edge [36].

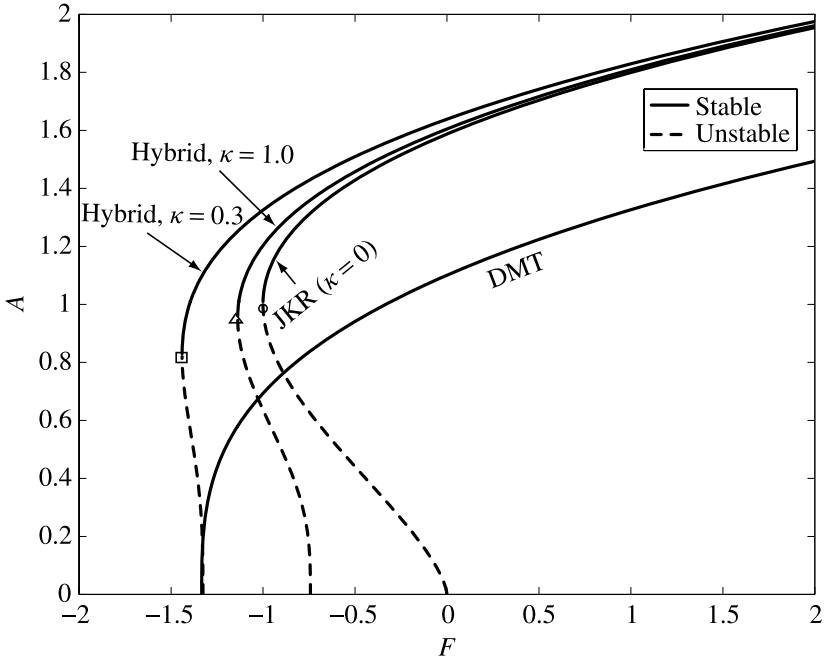

Figure 8. Comparison of the hybrid model with $\kappa = 0.1$ and 0.3, JKR and DMT model.

4. Instability Jump

The principal difference between the JKR and DMT models, as far as the pull-off process is concerned, is that the JKR model predicts a sudden separation at a finite contact radius, whereas the DMT model predicts a continuous separation at point contact as shown in Fig. 8. This sudden jump-off phenomenon is observed in the experiment of soft rubber contact [5] as well as for hard mica [8], also in the numerical computation of the self-consistent method [25, 26, 30]. However, this jump-off phenomenon is inconsistent with the viewpoint of fracture mechanics. When the external compression load reduces (or tension increases), the contact radius reduces, which is viewed as a crack propagation process starting from the contact edge towards the center [24, 32, 33]. The crack propagation should proceed in a continuous way [31, 32], which is the case predicted by the DMT and Hertz models. However, the crack propagation may not be the only mechanism causing the separation. Pashley [36] points out that the jump-off phenomenon in the cases with large Tabor numbers (the quintessential JKR system) arises from the sharp fall in the surface force as the contact area decreases and is not merely a result of the infinite tensile stress around the periphery, which is responsible for crack propagation. Therefore, surface deformation and crack propagation are the two mechanisms driving the separation. For the JKR system with its large adhesion and compliant-body, the surface is prone to deform, and the changed surface interaction forces, together with the tensile pressure around periphery, can cause jump-off; for the DMT system with

its small-adhesion and hard-body, the crack propagation mechanism dominates and the separation occurs in a continuous way. Based on the contact pressure profile analysis, two new jumps are proposed here. One jump leads to the transition of the JKR model to the DMT model and the other leads to the flaw-insensitive failure mode [24, 32, 33]. Unlike jump-off, the two jumps proposed here do not lead to a total separation of two contacting bodies.

Here r_0 is defined as the radial distance where the JKR pressure vanishes, i.e., $p(r_0) = 0$. From equation (5), r_0 is found as follows:

$$r_0 = a\sqrt{1 + p_0'/p_0}. \tag{29}$$

As shown in Fig. 9, $p(r)$ is in compressive mode when $r < r_0$ and $p(r)$ is in tensile mode when $a > r > r_0$. As for the JKR model, substitute $p_0 = 2Ea/(\pi R)$ and $p_0' = -\sqrt{4E\gamma/(\pi a)}$ into equation (29) and then nondimensionalize it. The following dimensionless form of equation (29) is obtained:

$$R_0 = A\sqrt{1 - \frac{2}{3}A^{-3/2}}, \tag{30}$$

where $R_0 = r_0/a_c$. For R_0 to be real, the item inside square root must be nonnegative, therefore

$$A \geqslant (3/2)^{-2/3}. \tag{31}$$

Hence we define $A_{\min} = (3/2)^{-2/3} \approx 0.763$. Clearly, if $A < A_{\min}$, R_0 does not exist in the real domain. Figure 9 plots the A–R_0 curve of equation (30) together with a straight line of $R_0 = A$. In Fig. 9, the pressure of the zone between the straight line and the $R_0 = A\sqrt{1 - \frac{2}{3}A^{-3/2}}$ curve which physically corresponds to the annulus zone of $a > r > r_0$, is tensile; the pressure of the zone below the $R_0 = A\sqrt{1 - \frac{2}{3}A^{-3/2}}$ curve (the circular zone of $r < r_0$) is compressive. Clearly, if $A < A_{\min}$ and two bodies are still in contact, the JKR demarcation of tensile and compressive zones inside the contact region can no longer exist. Logically, only two scenarios are left for choice: either the whole contact pressure becomes compressive (as in the case of the Hertz and DMT models) or the whole contact pressure becomes tensile.

Figure 10 plots the surface interaction force per unit area, σ of equation (3), as a function of separation distance z and three contact scenarios. The term z_0 is the equilibrium separation distance, i.e., $\sigma(z_0) = 0$; z_1 is the separation distance where the maximum attractive σ is reached, i.e., $\sigma(z_1) = \sigma_0$ and $z_1 = 1.255z_0$ as discussed before. Figure 10(a) is the JKR contact scenario: the separation distance of the central parts is less than z_0, which is in the repulsive zone of σ and this leads to a compressive contact pressure; the separation distance of the peripheral parts are larger than z_0 and therefore, the attractive σ induces a tensile contact pressure. Figure 10(a) was originally given by Tabor [11] and here the neck height is exaggerated in the plot. Figure 10(b) is the Hertz/DMT contact scenario: the

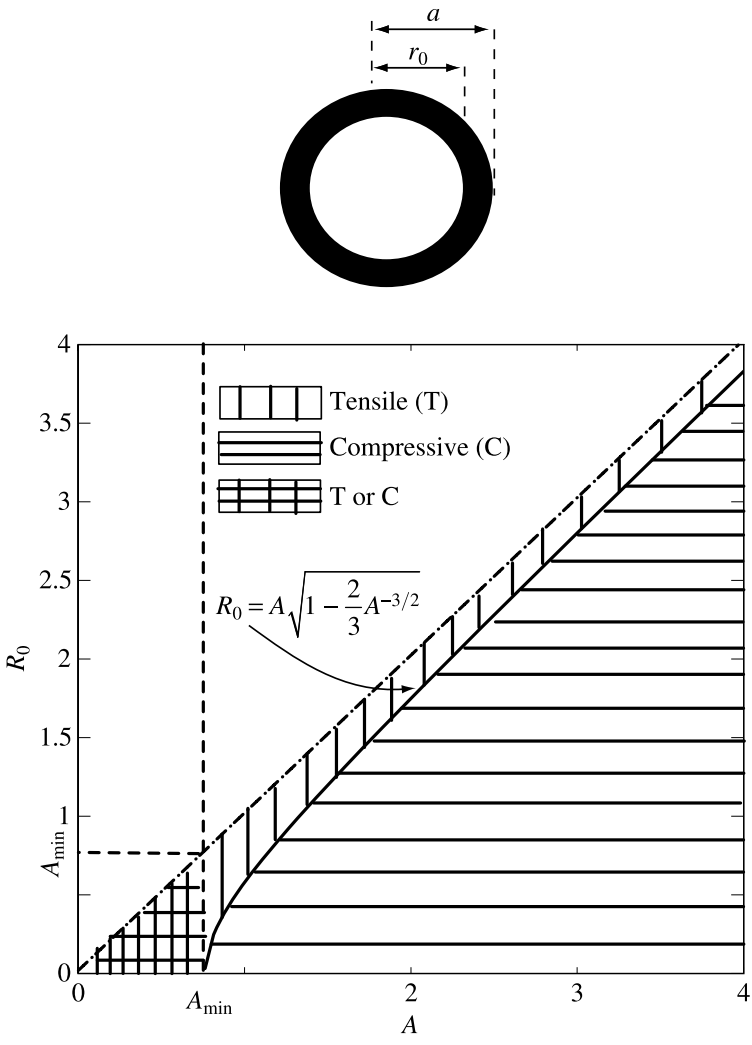

Figure 9. Definition of r_0 and A–R_0 plot.

separation of whole contact region is less than z_0 and the repulsive σ induces a compressive contact pressure in the whole contact area. The neck height is also reduced in Fig. 10(b) for the DMT model. Figure 10(c) is the scenario that all the contact pressure is tensile. The whole contact region is in the attractive zone of $z > z_0$. In general, the contact surface profiles are still curved ones (as indicated by dashed line). The limit case is that the whole contact region becomes a cohesive zone where the contact pressure is a constant of $p = \sigma_0$; the whole contact region becomes flat with a constant separation distance of z_1 as indicated by a solid line. For $p = -\sigma_0$ is the maximum tensile contact pressure that the contacting bodies can bear, further increasing the external tensile load will result in an abrupt jump-off, which is the flaw-insensitive failure mode [24, 32, 33]. The difference between

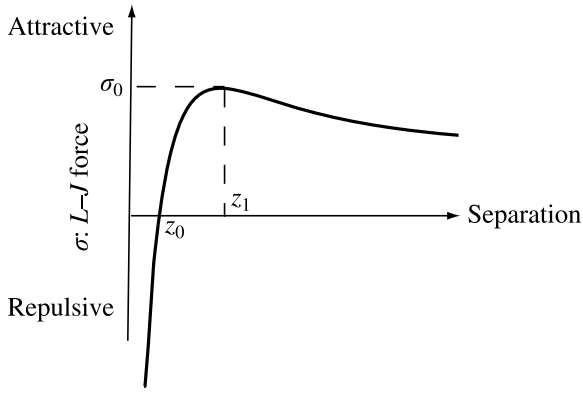

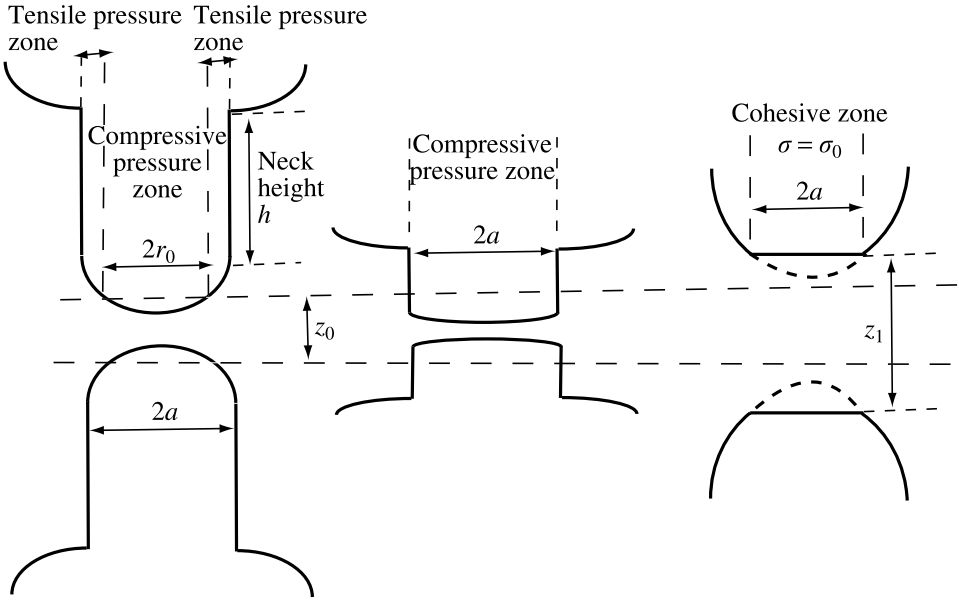

(a) JKR pressure, $A > A_{\min}$ (b) Hertz pressure, $A < A_{\min}$ (c) Tensile pressure, $A < A_{\min}$

Figure 10. Surface force per unit area of LJ potential as a function of the separation distance z and three contact scenarios: (a) the JKR contact pressure profile: the central parts are compressive and the peripheral parts are tensile; (b) Hertz/DMT pressure profile: compressive pressure over all the contact region; (c) Tensile pressure over all the contact region.

our second jump scenario and the flaw-insensitive failure mode should be emphasized here. The dimensionless parameter used to indicate the flaw-sensitive and flaw-insensitive regimes is $[\gamma E/(R_{\text{cyl}}\sigma_0^2)]^2$ (R_{cyl} is the cylinder radius) by Gao *et al.* [24] and $\sigma_0 R_{\text{cyl}}/(2\pi E\delta_{\text{c}})$ (δ_{c} is the critical separation distance) by Hui *et al.* [32]. For a given system, Gao and Hui's dimensionless parameters will tell whether the crack propagation failure mode (flaw-sensitive) or the jump-off failure mode

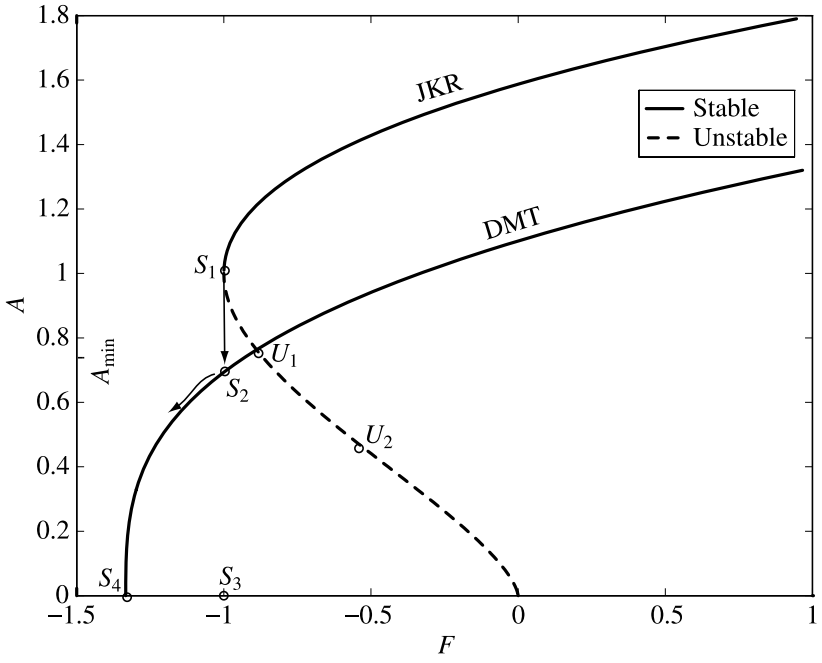

Figure 11. Jump phenomenon: the JKR curve loses stability at S_1 $(-1, 1)$ when external loading force P is a control parameter. Instead of jumping directly to S_3 $(-1, 0)$, there is an alternative to jump from S_1 to S_2 $(-1, 0.69)$ on the DMT curve and follow through to the separation of S_4 $(-4/3, 0)$. U_1 $(-0.89, 0.763)$ is the point below which in the JKR model the tensile contact pressure can no longer exist and it is also the intersection of the JKR and DMT curves. U_2 $(-5/9, 0.481)$ is the instability point when δ is the control parameter.

(flaw-insensitive), occurs. Our second jump is applied to such scenario: at the beginning, the contact radius reduces as the crack propagation failure mode until the JKR pressure pattern can no longer exist; and then the contacting surfaces jump into the attractive zone; if the external tensile load is further increased, the jump-off failure mode occurs. In short, our second jump is a transition from the flaw-sensitive failure mode to the flaw-insensitive failure mode.

Figure 11 plots the jump from the JKR curve to the DMT curve. Here the state variable expression [49] for the points in Fig. 11 is used. For example, $S_1 = S_1$ $(-1, 1)$ is the JKR pull-off point when the external load F is the controlling parameter [21] and U_1 $(-0.89, 0.763)$ $(A_{\min} = 0.763)$ is the critical point below which, as analyzed above, the JKR pressure profile cannot exist. It should be noticed that U_1 is the intersection point of the JKR curve and the DMT curve because the DMT model assumes no tensile contact pressure [19]. Because there is a gap between S_1 and U_1, we propose the following jump: instead of a jump of total separation from S_1 to S_3 $(-1, 0)$, the jump from S_1 to S_2 $(-1, 0.69)$ on the DMT curve occurs, and then follows the DMT curve until the final separation of the contact point at S_4 $(-4/3, 0)$. This new jump scenario of S_1 to S_2 is similar to the mode jumping

scenario of a buckled beam on a nonlinear elastic foundation, in which the modal amplitudes at a fixed load jump to other finite values instead of reducing to zero [49]. Here we emphasize that this new jump occurs as the external load F is the controlling parameter. If the approach distance δ is the controlling parameter, the instability of the JKR model occurs at U_2 $(-5/9, 0.481)$ [21], not S_1. The jump from S_1 to S_2, which occurs under a tensile external load, corresponds to the jump scenario from Fig. 10(a) to 10(b). The S_1 to S_2 jump reduces the contact radius a (A) and causes the whole contact pressure to become (compressive) Hertzian. At S_2, the compressive elastic restoring force due to the compressive contact pressure by no means balances the tensile external load and the attractive surface force outside the contact region must be brought in to balance the tensile external load. Therefore, the S_1 to S_2 jump also induces the surface profile change: the neck height (dramatically) reduces as schematically plotted in Fig. 10(a) and 10(b). Because the above instability jump analysis is based on the JKR pressure of equation (5), it is also possible in the real world to have a smooth transition as shown in Fig. 12, instead of an instability jump. The JKR model applies in the range of $\mu > 5$ and the DMT model applies in the range of $\mu < 0.1$. A MD curve with the intermediate range of μ can intersect the DMT curve at U_1. Instead of following the total separation route of jumping from U_1 to S_5, the MD curve may smoothly transit to the DMT curve and then follow the DMT curve to the final separation at S_4. In general, the jump from

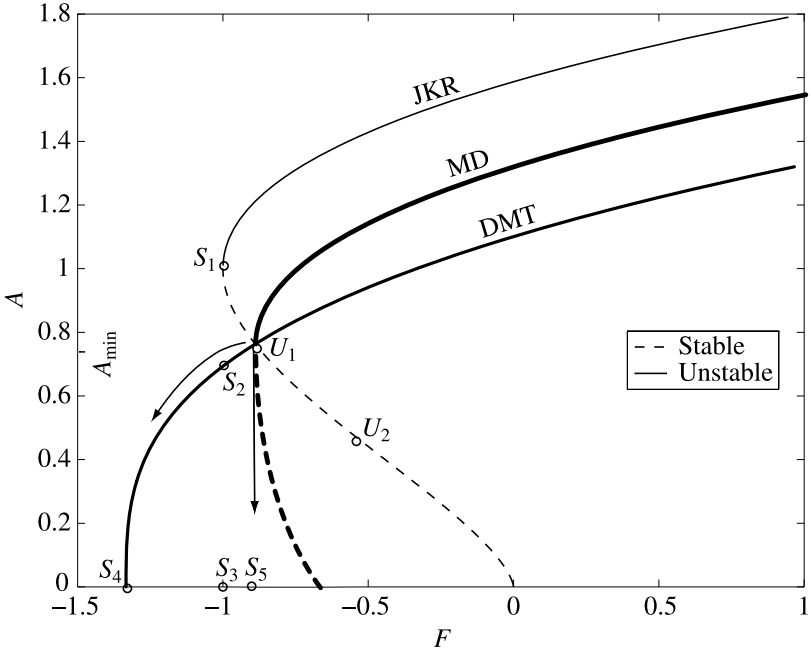

Figure 12. The scenario of smooth transition between the MD and DMT models. In this scenario that the instability point of MD model coincides with U_1, the MD curve will smoothly transit to the DMT curve instead of jumping from U_1 to S_5.

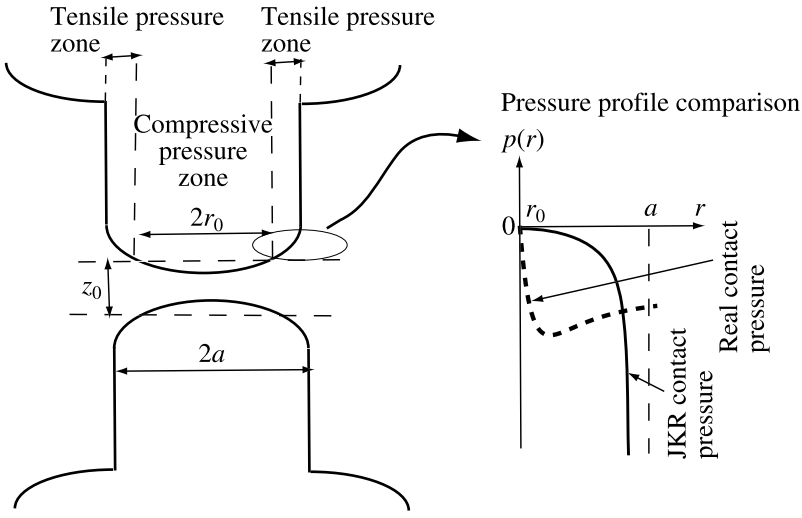

Figure 13. The comparison of the contact pressure profiles: the JKR contact pressure and the real contact pressure (as observed in the self-consistent methods).

the MD model to the DMT model is less dramatic. The contact pressure difference between the MD model and JKR model is that the maximum tensile pressure of σ_0 is reached in a peripheral annulus of the cohesive zone in the MD model; whereas the JKR pressure approaches infinity, unrealistically, at the contact edge as shown in Fig. 13. The real pressure profile at the contact periphery, as computed by the self-consistent methods [25, 26, 30], is also demonstrated schematically in Fig. 13 as a dashed line. Instead of going to infinity as does the JKR pressure, the real pressure reaches a maximum and then reduces rapidly approaching zero as the radial distance r increases.

There are several instability and hysteresis jumps shown by Greenwood (e.g., in his Fig. 2(a)) [30]. However, none of Greenwood's jumps correspond to our jump because in Greenwood's jump study, the approach distance δ is the controlling parameter and jumps occur with the change of external load. The P–δ curve presented in the self-consistent methods and δ used as the controlling parameter [25–27, 30] makes it very difficult, if not impossible, for us to find the direct evidence in the numerical computation of the self-consistent method to corroborate the newly proposed jump scenario. The slowly varying deformation assumption used in the self-consistent method [25] may also disguise the jump because there must be a sudden surface profile change accompanying this S_1 to S_2 jump, as analyzed above. The difference between the JKR pressure and the real one may also make this instability jump less obvious in the self-consistent method. At the same time, observing the jump, experimentally, from S_1 to S_2 may be very difficult because of the transient effect induced by the jump. All our contact analyses here are static ones and the dynamic transient effect can cause a significant deviation to the static theory from the experimental observation in a micro-structure instability jump study [50].

Due to the dynamic transient effect, the contact bodies may not be able to jump from S_1 to S_2 and then stay on the DMT curve. Instead, the contacting bodies will have a total separation as observed in the JKR experiments [5]. Nevertheless, this new jump scenario offers an explanation for the experimental observations by Israelachvili *et al*. [29] that the JKR model better describes the surface deformation of contacting bodies before pull-off and the DMT model gives a more accurate pull-off force value. Again, keep in mind that all of the classical hard contact models fail to capture the abrupt contact surface profile change just before pull-off [25, 26]. The introduction of this new jump in essence is to capture such a change, which may serve as a guide for a more refined study of self-consistent methods in the future.

In an analysis of a self-consistent method very similar to our equation (30), Muller, Yushchenko and Derjaguin have foreseen the scenario of $r_0 = 0$ at $a \neq 0$ as a possibility without a detailed discussion [13]. When the scenario of $r_0 = 0$ at $a \neq 0$ occurs, Muller, Yushchenko and Derjaguin postulated that only the attractive forces act in the contact region [13], which induces only tensile contact pressure as shown in Fig. 10(c). In a self-consistent method, Feng [26] shows in his Fig. 5(b) that there is a pressure distribution (with $\mu = 0.01$) which becomes all tensile, whereas others obey the JKR pattern. Similarly, Attard and Parker [25] show that two pressure distributions with the largest positive h_0's become all tensile in their Fig. 6(c) and the others still keep the JKR pattern. Zhang [19] shows that the tensile contact pressure occupies more and more of the contact region when the contact radius is reduced. Also from Fig. 9, the slope of $R_0 = A\sqrt{1 - \frac{2}{3}A^{-3/2}}$ becomes steep around $A_{\min}$ and the limit case is that at $A = A_{\min}$ the contact pressure becomes all tensile. Again, if the external load P is the controlling parameter, there is a gap between S_1 and U_1, and there will be an instability jump for the JKR pressure pattern of Fig. 10(a) to become the all tensile pressure scenario of Fig. 10(c). While, if δ is the controlling parameter as in many self-consistent methods [25, 26, 30], U_2 is below U_1 and the smooth transition can thus be achieved. When the contact pressure becomes all tensile (i.e., large negative δ), both the contact radius and the forces due to elastic deformation are very small. The dominant forces are the attractive surface interaction forces and the Bradley model thus applies. This can offer an explanation for Greenwood's observation [30] that for the system with a fixed Tabor number ($\mu \geqslant 2$), the JKR model is applicable when δ is positive or slightly negative and the Bradley models are applicable when δ is large and negative.

It is also necessary for us to have a brief discussion on the jump-on phenomenon [26, 30]. In contrast to jump-off occurring in the separation process, jump-on occurs when two bodies approach each other. The contact equilibrium can be viewed as the elastic restoring force due to deformation balancing the combined effects of the surface interaction forces and external load [36]. The jump-on phenomenon is the same as the pull-in instability of micro-structures [50–52]. When two bodies approach each other, the attractive surface interaction forces increase nonlinearly and dramatically, which is the same scenario as seen when the van der Waals (vdW) force increases nonlinearly as the separation distance of two nanotubes reduces

[51]; or as the electrostatic force increases nonlinearly when the gap distance between the micro-structure and substrate decreases [50, 52]. When a critical point is reached, at which the elastic restoring force due to deformation can no longer balance the vdW or electrostatic force, the pull-in instability occurs: the structure experiences an abrupt snap-through jump to reach a new equilibrium. The jump-on phenomenon in contact mechanics is a pull-in instability jump at which the elastic restoring force cannot balance the nonlinearly increasing surface interaction forces.

5. Concluding Remarks

Johnson and Greenwood are very cautious to prescribe their adhesion map only in the compressive external load range [17]. Yao *et al*. extended Johnson and Greenwood's adhesion map to a tensile external load range by considering the adhesion strength [18]. However, in the small sign-changing range of external load (or δ or h_0), the surface profiles of two bodies have dramatic shape changes as observed in many self-consistent computations, which, as a result, causes the significant changes of the total surface energy and surface interaction forces. This is a major reason as to why the classical hard contact models fail in this small range, especially for the large-adhesion, compliant-body cases [25]. The self-consistent method also finds that in this small range, for a system with a fixed Tabor number, the JKR model is applicable in one portion and the DMT applicable in the other [30]. Therefore, when the range of external tensile load is included in the adhesion map, using the Tabor number (or equivalently, the elasticity number) and $\bar{P}$ ($\bar{P} = P/(\lambda\gamma R)$) only, it is not enough to demarcate the applicability ranges of different classical hard contact models. J, β and κ together with the two new jump scenarios are thus introduced to capture the significant surface deformation in that small sign-changing range and also provides a better approximation for the rigid-soft contact with a small contact radius. The introduction of J, β and κ establishes a new hybrid model and a framework to correlate different classical hard contact models. The hybrid model also provides the explanations for the differences between the self-consistent method, experimental data and the classical hard contact models. The adhesion map presented in our Fig. 2 systematically shows how different classical hard contact models relate and transit to one another by varying J, β and κ. At the same time, the physical meaning of varying the three parameters is also given. By doing this, we hope that this paper can offer, to readers, a helpful review of classical hard contact models as approached from a different angle.

Acknowledgements

This work is supported the NSFC Grant No. 10721202 and MOST Grant No. 2010CB631004.

References

1. H. Hertz, *J. rein und angwandte mathematik* **92**, 156 (1882). (For English translation see *Miscellaneous Papers*, H. Hertz (Ed.). Jones and Schott, Macmillan, London, UK (1896).)
2. R. S. Bradley, *Phil. Mag*. **13**, 853 (1932).
3. B. V. Derjaguin, *Kolloid Z.* **69**, 155 (1934).
4. J. N. Israelachvili, *Intermolecular and Surface Forces*. Academic Press, London, UK (1985).
5. K. L. Johnson, K. Kendall and A. D. Roberts, *Proc. Roy. Soc. London, Ser. A* **324**, 301 (1971).
6. B. V. Derjaguin, V. M. Muller and Yu. P. Toporov, *J. Colloid Interface Sci*. **53**, 314 (1975).
7. D. Tabor, *J. Colloid Interface Sci*. **67**, 380 (1975).
8. D. Tabor, *J. Colloid Interface Sci.* **73**, 294 (1979).
9. B. V. Derjaguin, V. M. Muller and Yu. P. Toporov, *J. Colloid Interface Sci*. **67**, 378 (1975).
10. B. V. Derjaguin, V. M. Muller and Yu. P. Toporov, *J. Colloid Interface Sci.* **73**, 293 (1979).
11. D. Tabor, *J. Colloid Interface Sci.* **58**, 2 (1977).
12. B. D. Hughes and L. R. White, *Quart. J. Mech. Appl. Math*. **32**, 445 (1979).
13. V. M. Muller, V. S. Yushchenko and B. V. Derjaguin, *J. Colloid Interface Sci*. **77**, 91 (1980).
14. V. M. Muller, V. S. Yushchenko and B. V. Derjaguin, *J. Colloid Interface Sci.* **92**, 92 (1983).
15. D. Maugis, *J. Colloid Interface Sci*. **150**, 243 (1992).
16. D. S. Dugdale, *J. Mech. Phys. Solids* **8**, 100 (1960).
17. K. L. Johnson and J. A. Greenwood, *J. Colloid Interface Sci*. **192**, 326 (1997).
18. H. Yao, M. Ciavarella and H. Gao, *J. Colloid Interface Sci*. **315**, 786 (2007).
19. Y. Zhang, *J. Adhesion Sci. Technol.* **22**, 699 (2008).
20. K. S. Kim, R. M. McMeeking and K. L. Johnson, *J. Mech. Phys. Solids* **46**, 243 (1998).
21. K. L. Johnson, *Contact Mechanics*. Cambridge University Press, Cambridge, UK (1985).
22. D. S. Rimai, L. P. DeMejo and W. B. Vreeland, *Langmuir* **10**, 4361 (1994).
23. D. S. Rimai, D. J. Quesnel and R. C. Bowen, *Langmuir* **17**, 6946 (2001).
24. H. Gao, X. Wang, H. Yao, S. Gorb and E. Arzt, *Mech. Mater*. **37**, 275 (2005).
25. P. Attard and J. L. Parker, *Phys. Rev. A* **46**, 7959 (1992).
26. J. Q. Feng, *Colloids and Surfaces A* **172**, 175 (2000).
27. J. Q. Feng, *J. Colloid Interface Sci.* **238**, 318 (2001).
28. L. E. Goodman and L. M. Keer, *Int. J. Solids Structures* **1**, 407 (1965).
29. J. N. Israelachvili, E. Perez and R. K. J. Tandon, *J. Colloid Interface Sci.* **78**, 260 (1980).
30. J. A. Greenwood, *Proc. Roy. Soc. London Ser. A* **453**, 1277 (1997).
31. G. I. Barenblatt, *Adv. Appl. Mech*. **7**, 55 (1962).
32. C. Y. Hui, N. J. Glassmaker, T. Tang and A. Jagota, *J. R. Soc. Lond. Interface* **1**, 35 (2004).
33. T. Tang, C. Y. Hui and N. J. Glassmaker, *J. R. Soc. Lond. Interface* **2**, 505 (2005).
34. E. Barthel, *J. Colloid Interface Sci.* **200**, 7 (1998).
35. V. M. Muller, B. V. Derjaguin and Y. P. Toporov, *Colloids Surf.* **7**, 251 (1983).
36. M. D. Pashley, *Colloids Surf.* **12**, 69 (1984).
37. J. A. Greenwood, *Phil. Mag*. **89**, 945 (2009).
38. J. J. Wu, *J. Phys. D: Appl. Phys.* **39**, 351 (2006).
39. C. Argento, A. Jagota and W. C. Carter, *J. Mech. Phys. Solids* **45**, 1161 (1997).
40. F. Q. Yang, *J. Mater. Res.* **21**, 2683 (2006).
41. A. A. Griffith, *Phil. Trans. R. Soc. London Ser. A* **221**, 163 (1920).
42. H. H. Yu and Z. Suo, *J. Mech. Phys. Solids* **46**, 829 (1998).
43. D. Maugis, *Langmuir* **11**, 679 (1995).
44. R. W. Carpick, D. F. Ogletree and M. Salmeron, *J. Colloid Interface Sci.* **211**, 395 (1999).

45. F. Q. Yang, X. Z. Zhang and J. C. M. Li, *Langmuir* **17**, 716 (2001).
46. R. G. Horn, J. N. Israelachvili and F. Pribac, *J. Colloid Interface Sci.* **115**, 480 (1987).
47. K. L. Johnson, *Langmuir* **12**, 4510 (1996).
48. D. Maugis and H. M. Pollock, *Acta metall.* **32**, 1323 (1984).
49. Y. Zhang and K. D. Murphy, *Int. J. Nonlinear Mech*. **40**, 795 (2005).
50. Y. Zhang, Y. Wang, Z. Li, Y. Huang and D. Li, *J. Microelectromech. Syst.* **16**, 684 (2008).
51. G. W. Wang, Y. Zhang, Y. Zhao and G. Yang, *J. Micromech. Microeng.* **14**, 1119 (2004).
52. Y. Zhang and Y. Zhao, *Sens. Actuators A* **127**, 366 (2006).